Advanced Myocardial MRI Tissue Characterization Combining Contrast Agent-Free T1-Rho Mapping With Fully Automated Analysis

Victor de Villedon de Naide, MSc,[1,2] Kalvin Narceau, MSc,[1] Valery Ozenne, PhD,[1] Manuel Villegas-Martinez, PhD,[1,2] Victor Nogues, MSc,[1] Nina Brillet, MSc,[1] Jana Huiyue Zhang, MSc,[3] Ilyes Benlala, PhD,[2] Matthias Stuber, PhD,[1,3,4] Hubert Cochet, MD, PhD,[1,2] and Aurélien Bustin, PhD[1,2,3*]

Background: Myocardial T1-rho (T1ρ) mapping is a promising method for identifying and quantifying myocardial injuries without contrast agents, but its clinical use is hindered by the lack of dedicated analysis tools.
Purpose: To explore the feasibility of clinically integrated artificial intelligence-driven analysis for efficient and automated myocardial T1ρ mapping.
Study Type: Retrospective.
Population: Five hundred seventy-three patients divided into a training (N = 500) and a test set (N = 73) including ischemic and nonischemic cases.
Field Strength/Sequence: Single-shot bSSFP T1ρ mapping sequence at 1.5 T.
Assessment: The automated process included: left ventricular (LV) wall segmentation, right ventricular insertion point detection and creation of a 16-segment model for segmental T1ρ value analysis. Two radiologists (20 and 7 years of MRI experience) provided ground truth annotations. Interobserver variability and segmentation quality were assessed using the Dice coefficient with manual segmentation as reference standard. Global and segmental T1ρ values were compared. Processing times were measured.
Statistical Tests: Intraclass correlation coefficients (ICCs) and Bland–Altman analysis (bias ±2SD); Paired Student's *t*-tests and one-way ANOVA. A *P* value <0.05 was considered significant.
Results: The automated approach significantly reduced processing time (3 seconds vs. 1 minute 51 seconds ± 22 seconds). In the test set, automated LV wall segmentation closely matched manual results (Dice 81.9% ± 9.0) and closely aligned with interobserver segmentation (Dice 82.2% ± 6.5). Excellent ICCs were achieved on a patient basis (0.94 [95% CI: 0.91 to 0.96]) with bias of $-0.93\ cm^2 \pm 6.60$. There was no significant difference in global T1ρ values between manual (54.9 msec ± 4.6; 95% CI: 53.8 to 56.0 msec, range: 46.6–70.9 msec) and automated processing (55.4 msec ± 5.1; 95% CI: 54.2 to 56.6 msec; range: 46.4–75.1 msec; $P = 0.099$). The pipeline demonstrated a high level of agreement with manual-derived T1ρ values at the patient level (ICC = 0.85; bias +0.52 msec ± 5.18). No significant differences in myocardial T1ρ values were found between methods across the 16 segments ($P = 0.75$).
Data Conclusion: Automated myocardial T1ρ mapping shows promise for the rapid and noninvasive assessment of heart disease.
Evidence Level: 3
Technical Efficacy: Stage 1

J. MAGN. RESON. IMAGING 2025;61:1353–1365.

View this article online at wileyonlinelibrary.com. DOI: 10.1002/jmri.29502

Received Apr 11, 2024, Accepted for publication Jun 10, 2024.

*Address reprint requests to: A.B., Hôpital Xavier Arnozan, Avenue du Haut-Léveque, Pessac 33604, France. E-mail: aurelien.bustin@ihu-liryc.fr

From the [1]IHU LIRYC, Electrophysiology and Heart Modeling Institute, Université de Bordeaux, INSERM, Centre de Recherche Cardio-Thoracique de Bordeaux, U1045, Pessac, France; [2]Department of Cardiothoracic Imaging, Hôpital Cardiologique du Haut-Lévêque, CHU de Bordeaux, Pessac, France; [3]Department of Diagnostic and Interventional Radiology, Lausanne University Hospital and University of Lausanne, Lausanne, Switzerland; and [4]Center for Biomedical Imaging (CIBM), Lausanne, Switzerland

Additional supporting information may be found in the online version of this article

Myocardial T1-rho (T1ρ) mapping is a promising endogenous biomarker for detecting and quantifying myocardial injuries, offering distinct advantages over conventional contrast-enhanced methods.[1] This noninvasive imaging technique does not require the injection of contrast agents, making it a "needle-free" and cost-effective diagnostic marker that may potentially have high impact both in terms of clinical outcomes and patient comfort.[2,3]

One specific application that showcases the potential impact of T1ρ mapping lies in patients with kidney failure, who currently face limitations in receiving gadolinium-based contrasts due to compromised kidney function.[4] These patients represent 49% of the heart failure population.[5] By enabling fibrosis assessment in this patient group, T1ρ mapping may address an important unmet need and may thus contribute to improved clinical outcomes.[6] The simplicity of this technique facilitates patient management and promotes serial MRI screening to monitor disease progression effectively, including screenings for vulnerable populations such as children and pregnant women.

However, despite the promise of T1ρ mapping, its clinical adoption has been hindered by a lack of dedicated post-processing software and efficient analysis tools.[7] Imagers currently rely on time-consuming visual assessments and labor-intensive manual segmentation of endocardial and epicardial borders, along with the positioning of insertion points to generate the American Heart Association (AHA) 16-segment model, as recommended by recent guidelines from the Society for Cardiovascular Magnetic Resonance (SCMR) on parameter mapping.[8] Unfortunately, these manual inputs not only burden imagers but also introduce operator variability, potentially compromising the accuracy and reliability of results.[9]

Drawing from experience with other parameter mapping techniques, such as T1 and T2 mapping,[10,11] we posit that an artificial intelligence (AI)-driven analysis can improve the assessment of myocardial T1ρ maps. We hypothesized that AI would allow faster, easier, and more efficient analysis, with the potential to eliminate error-prone manual processes. This could potentially be an important step toward the widespread clinical adoption of this imaging technique.

Thus, the aim of this study was to explore the feasibility and evaluate the accuracy, reliability, and diagnostic performance of clinically integrated AI-driven analysis for myocardial T1ρ mapping, using manual analysis as the reference standard.

Materials and Methods

This retrospective study was approved by our Institutional Ethics Committee and all patients provided informed consent for this particular study.

Description of the Study Participants

Between July 2020 and July 2021, 73 patients (testing set, median age [Q1–Q3], 55 years [41–66], 32 female) with suspected heart disease who underwent MRI and myocardial T1ρ mapping at Bordeaux University Hospital were enrolled in this study. The training set comprised a distinct group of 500 patients (median age [Q1–Q3], 63 years [55–71], 110 female) with suspected ischemic structural heart disease, who underwent T1ρ-weighted imaging and who were concurrently enrolled in a separate study from March 2021 to July 2023. Figure S1 in the Supplemental Material outlines the study's flowchart. The inclusion criterion was a clinical indication for contrast-enhanced cardiac MRI as part of standard care. Exclusion criteria included age < 18-year-old, history of allergic reactions to gadolinium-based contrast agents, severe renal failure, presence of a non-MR-conditional implantable device, inability to maintain a supine position for 50 minutes, pregnancy, breastfeeding, and inability to provide informed consent. Patient inclusion was not continuous as it depended on clinical workflow and was influenced by concurrent research projects involving similar patient cohorts.

Baseline patient characteristics are detailed in Table 1. The study population encompassed 477 ischemic patients, 64 non-ischemic patients, and 32 negative-MRI subjects. The training set, consisting of 500 patients, showed significant differences compared to the testing set, in terms of age (63 years-old [55–71] vs. 55 years-old [41–66]), prevalence of hypertension (42% vs. 12%), dyslipidaemia (44% vs. 7%), diabetes mellitus (44% vs. 7%), and troponin levels (1025 pg/mL [656–2059] vs. 187 pg/mL [39–846]). The ejection fraction determined by MRI was significantly lower in the training set compared to the testing set (40 ± 13% vs. 49 - ± 14%). No significant differences were observed in heart rate ($P = 0.32$), body mass index ($P = 0.10$), or gender ($P = 0.17$) between the two cohorts.

MR Imaging

MRI acquisitions were performed in the supine position on a 1.5-T clinical scanner (MAGNETOM Aera, Siemens Healthcare, Erlangen, Germany) with a 32-channel spine coil and a dedicated 18-channel body coil.

2D MYOCARDIAL T1ρ MAPPING SEQUENCE. The 2D myocardial T1ρ mapping sequence (Fig. 1) involved the acquisition of T1ρ maps using a breath-held motion-corrected balanced steady-state free-precession (bSSFP) sequence, which incorporates an adiabatic T1ρ preparation module to achieve T1ρ weighting.[12] Five T1ρ-weighted images with varying spin-lock times (TSL = [0, 10, 20, 35, 50] msec) were collected sequentially in the mid-diastolic phase during 13 heartbeats. A pause of two heartbeats between spin-lock acquisitions was employed to facilitate full magnetization recovery. Three short-axis slices (basal, middle, and apical) were acquired for each study participant. Acquisition parameters are outlined in Table S1 in the Supplemental Material, and further explanation of the sequence can be found in Bustin et al.[12]

TESTING SET. The MRI protocol followed conventional SCMR guidelines, including cine bSSFP imaging in 2-, 3-, and 4-chamber views, and in a series of contiguous short-axis slices spanning the ventricles. Breath-held 2D myocardial T1ρ maps were acquired

TABLE 1. Baseline Patient Characteristics for the Training and Testing Sets

	Training Set	Testing Set	*P*-Value
Data			
Number of participants	500	73	-
Time period	March 2021–July 2023	July 2020–July 2021	-
Number of images for analysis	6380	219	-
Number of T1ρ maps	0	219	-
Demographics			
Female gender	110 (22)	23 (32)	0.17
Age, years	63 [55–71]	55 [41–66]	<0.001*
Weight, kg	77 ± 16	75 ± 16	0.14
Height, cm	178 ± 63	172 ± 10	0.54
BMI, kg/m^2	26 ± 5	25 ± 5	0.10
Risk factors			
Hypertension	210 (42)	9 (12)	0.006*
Dyslipidaemia	220 (44)	5 (7)	<0.001*
Diabetes mellitus	140 (28)	3 (4)	0.02*
Smoking	285 (57)	18 (25)	0.14
Obesity (BMI ≥30 kg/m^2)	120 (24)	9 (12)	0.69
Family history of coronary artery disease	80 (16)	8 (11)	0.98
Cardiovascular markers			
Resting heart rate, beats/min	69 [56–76]	64 [57–73]	0.32
Systolic blood pressure, mm Hg	121 [111–133]	128 [110–133]	0.75
Diastolic blood pressure, mm Hg	73 [64–80]	74 [68–84]	0.47
NT-proBNP, pg/mL	1025 [656–2059]	187 [39–846]	0.02*
AF/atrial flutter	70 (14)	3 (4)	0.12
MRI function			
LVEDVi, mL/m^2	106 ± 30	101 ± 32	0.39
LVESVi, mL/m^2	66 ± 33	54 ± 34	0.035*
LVEF, %	40 ± 13	49 ± 14	<0.001*
LVEF impairment (LVEF <35%)	27 (37)	10 (14)	0.05
RVEDVi, mL/m^2	74 ± 20	84 ± 21	0.004*
RVESVi, mL/m^2	37 ± 17	42 ± 16	0.08*
RVEF, %	50 ± 11	50 ± 11	0.82
Post-MRI diagnoses			
Negative MRI	16 (3)	16 (22)	<0.001*
Ischemic heart disease	464 (93)	13 (18)	<0.001*
Nonischemic heart disease	20 (4)	44 (60)	<0.001*

Values are N (%) for categorical variables and mean ± SD or median [interquartile range] for continuous variables. AF = atrial fibrillation; BMI = body mass index; LV = left ventricle; LVEDVi = indexed left ventricular end-diastolic volume; LVESVi = indexed left ventricular end-systolic volume; LVEF = left ventricular ejection fraction; RVEDVi = right ventricular end-diastolic volume; RVESVi = right ventricular end-systolic volume; RVEF = right ventricular ejection fraction. Data are mean ± SD for continuous variables and number of patients for categorical variables. Data in parentheses are percentages.
*Significant difference between training and testing sets.

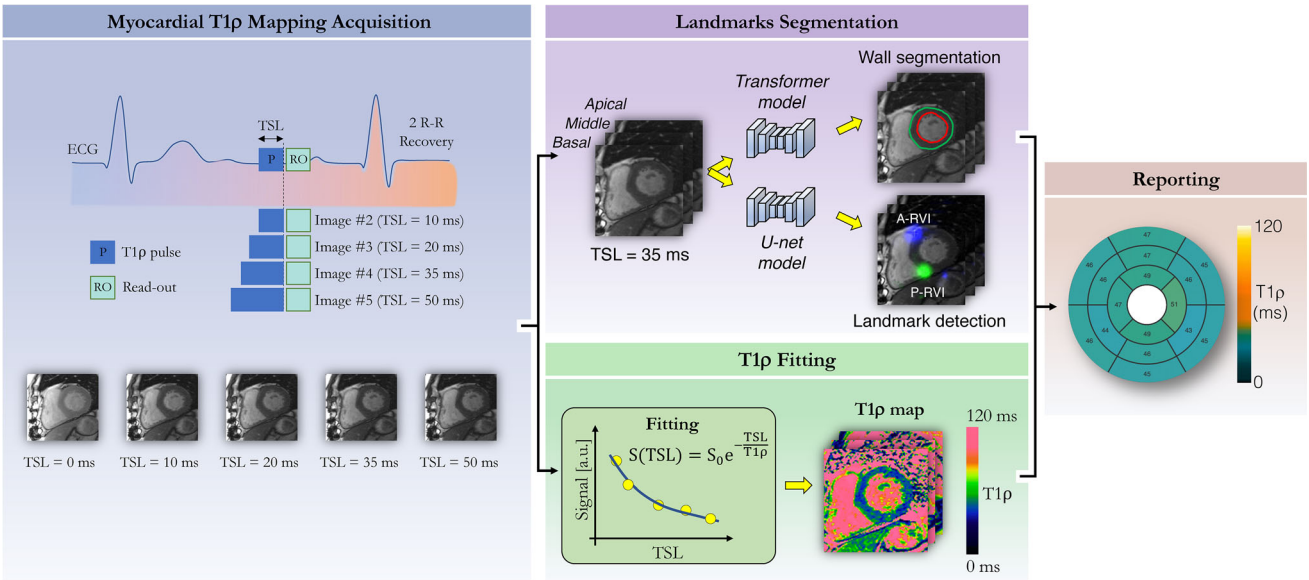

FIGURE 1: Diagram of the proposed pipeline for fully automated myocardial T1ρ mapping. Left: T1ρ mapping is performed using a single-shot electrocardiogram-triggered balanced steady-state free precession acquisition. This process acquires five images with varying spin lock times (TSL) over the span of 13 heartbeats within a single breath-hold. Middle: Leveraging a transformer-based model to achieve automated left ventricular wall segmentation in T1ρ images, alongside a U-Net architecture for the automated identification of the two right ventricular insertion points. Right: The pipeline automatically generates a 16-segment American Heart Association Bullseye model report.

before contrast administration following cine imaging. Three short-axis slices were collected (basal, middle, and apical) in each patient resulting in a total of 219 T1ρ maps. Late gadolinium enhancement (LGE) imaging was performed 15 minutes after the administration of 0.2 mmol/kg gadoteric meglumine (Dotarem, Guerbet, France), employing a breath-held phase-sensitive inversion recovery sequence[13] to collect a short-axis stack of contiguous slices covering the ventricles. Inversion times were adjusted to null viable myocardium.

TRAINING SET. These patients underwent a clinical protocol that included contrast-enhanced imaging with an additional pre-contrast breath-held 2D whole-heart T1ρ-weighted scan with TSL_{35} only (comprising 6380 images). This dataset was split into a training (85%) and a validation (15%) set used for U-Net-based landmark detection and Transformer-based LV segmentation. There was no overlap between the testing dataset and the training/validation data, ensuring the independence of test data. Training was conducted on a dedicated workstation with Intel Xeon Gold 6154, 3 GHz, 18 cores, 36 threads, NVIDIA Tesla V100 32 Go GPU, 377 GB RAM, Python version 2.7.18, Ubuntu Linux 18.04.6 LTS, CUDA 11.6, and TensorFlow 2.8.0.

Data Processing

AUTOMATED TRANSFORMER-BASED LEFT VENTRICULAR SEGMENTATION. A transformer-based model for medical image segmentation, inspired by Dosovitskiy et al,[14] was employed. A detailed description of the architecture can be found in Gao et al.[15] It is based on a hybrid approach to semantic segmentation, leveraging both the power of convolutional filters, and their ability to extract local features, with the advantages of vision transformers. The inclusion of attention maps helps the network to be less dependent on local space features. Images are first divided into patches, which are then embedded using a convolutional encoder. In each downsampling block, the embedding is downsampled and processed using a bi-directional transformer block. Similarly, each upsampling block performs the same operations, in an upsampling manner. At every scale, semantic maps, derived from the bi-directional multi-head attention block in the transformer, are extracted. These maps are then fused together using a multi-scale fusion process and skip connections to maintain high-level information that could have been lost during the downsampling phase. The final embeddings are then decoded using a convolutional decoder to output the segmentation map. This architecture is extremely data efficient and has shown excellent performance on medical datasets, especially when lowering the quantity of training examples, making it suitable for our needs, where data availability is low.[16] To alleviate partial volume effect on T1ρ values, the output myocardium contours were systematically eroded by one pixel.[17]

Adaptation to the current application. The settings were mostly replicated from Gao et al.[15] Data augmentation was used to avoid overfitting and included random rotations, flips, contrast adjustment, sharpness adjustment and Rician noise addition. The following parameters were used: equally weighted binary cross-entropy and dice loss, learning rate 10^{-3}, cropped 160 × 160 pixels TSL = 35 msec (TSL_{35}) image as input, binary left ventricular (LV) wall as output, normalization to zero mean and standard deviation of one. The model was trained using the AdamW optimizer for 77 epochs with a batch size of 8 and weight decay of 0.01.

RIGHT VENTRICULAR INSERTION POINTS DETECTION AND AHA's 16-SEGMENT MODEL CREATION. A conventional U-net-based method[18,19] was employed to automatically

locate the anterior and posterior right ventricular insertion points within short-axis TSL_{35} images. The SoftMax activation function was applied to obtain confidence scores, representing the probability of accurate landmark detection. Confidence calibration assesses the model's ability to provide precise correctness probabilities for predictions. The same hyperparameters described above were employed, except for the pixel-wise Euclidean distance loss and a base learning rate of 10^{-4}. To define segments within a cardiac level, both anterior and posterior right ventricular insertion points were used to establish two major axes.[20,21] For the basal and mid-cavity levels, the septal and lateral areas were further divided into six segments using an equiangular line. Finally, a 16-segment AHA bullseye model was created by incorporating both landmarks and LV contours.

INLINE INTEGRATION FOR PROSPECTIVE STUDIES. To assess the practical utility of the proposed framework in a clinical hospital environment, an inline point-of-care implementation of the pipeline was seamlessly integrated onto a clinical 1.5-T MRI scanner (MAGNETOM Aera, Siemens Healthcare, Erlangen, Germany) using the Gadgetron framework.[22] Model inference was conducted on a workstation equipped with an Intel Xeon CPU E5-2698 v4, 2.20 GHz, with 20 cores, 40 threads, NVIDIA Tesla K80 GPU, 512 GB RAM, Python 2.7.18, Ubuntu Linux 20.04.6, CUDA 11.4, TensorFlow 2.9.1, and Gadgetron 4.1.1. Native T1ρ-weighted images and their corresponding T1ρ maps were transmitted back to the user interface. These images were enriched with overlaid LV contours, AHA 16-segment bullseyes (displaying both mean and standard deviation), right ventricular insertion points, and associated confidence scores. Video S1 highlights the inline application of the proposed tool. The codes employed for training the segmentation and landmark models, the pre-trained models, and the Gadgetron gadgets are readily available to the community at the following repository: https://github.com/AurelienBustin/Automated-myocardial-T1-rho-mapping.

STANDARD OF REFERENCE. In the training set, three annotators, with 20, 20, and 15 years of experience in MRI image segmentation, performed the manual delineation of the endocardial and epicardial contours, as well as identifying right ventricular insertion points. Each annotator segmented a third of the dataset. The annotations were performed using CVI42 (Circle Cardiovascular Imaging, Calgary, Canada). For the testing set, the standard of reference was established by two radiologists (H.C. and S.S., with 20 and 7 years of MRI experience, respectively). These observers were entirely blind to the output of the algorithms and were unaware of the labels provided by other observers. One of the radiologists (S.S) independently re-annotated a subset of 47 patients from the testing set during a second session conducted over a month after the initial annotation. Myocardium contours were systematically eroded by one pixel.

Statistical Analysis

Statistical analysis was performed using SPSS Statistics v28 (IBM Corp., Armonk, NY). The Shapiro–Wilk test was used to test the null hypothesis that each continuous variable follows a normal distribution. Continuous variables are presented as mean ± SD (normally distributed) and as median [interquartile range Q1–Q3] (non-normally distributed). Categorical variables are presented as fraction (%). Parametric (unpaired Student's *t*-test) or non-parametric tests (Mann–Whitney) were used for continuous variables based on normality. Categorical variables were compared using χ^2 or Fisher's exact test as needed.

SEGMENTATION AND LANDMARKS QUALITY. The Friedman test was used to compare LV wall volumes obtained by the radiologists and the automated pipeline. Inter- and intraobserver reproducibility was assessed using Bland–Altman analysis and intraclass correlation coefficient (ICC) with 95% confidence interval (CI). Agreement was considered poor, moderate, good, or excellent for ICC <0.50, 0.50 to 0.75, 0.75 to 0.90, and >0.90.[23] One-way repeated measures analysis of variance (ANOVA) was used to compare Dice coefficients,[24] Jaccard index,[25] and center of mass difference between slices, followed by Tukey's post-hoc test for multiple comparison. Wilcoxon signed rank test assessed differences in Euclidian distance (mm) and insertion points angle (degrees) between anterior and posterior right ventricular insertion points. For each patient, the size of the 16 regions-of-interest (ROI) from the AHA model was documented for both manual and automated processing, and a comparison was conducted using a paired *t*-test. Processing times were measured and recorded.

MYOCARDIAL T1ρ VALUES COMPARISON. Paired Student's *t*-tests were used to compare automated and manual global T1ρ values. One-way ANOVA followed by Tukey's post-hoc test assessed regional T1ρ differences between slices and between AHA segments. Agreement in T1ρ values obtained with automated and manual processing was evaluated at patient, slice, and segment levels using Bland–Altman analysis and ICC with 95% CI, with agreement ranges as above. Sensitivity, specificity, positive and negative predictive values, and diagnostic accuracy of automated processing in detecting abnormal T1ρ values were calculated at patient, slice, and segment levels. Abnormal T1ρ values were defined as T1ρ ≥ 55 msec, based on mean + 2 SDs from a prior study on healthy volunteers at 1.5-T.[12] Myocardial T1ρ values on all true positive ($T1\rho_{Automated} \geq 55$ msec, $T1\rho_{Manual} \geq 55$ msec), true negative ($T1\rho_{Automated} < 55$ msec, $T1\rho_{Manual} < 55$ msec), false positive ($T1\rho_{Automated} \geq 55$ msec, $T1\rho_{Manual} < 55$ msec), and false negative ($T1\rho_{Automated} < 55$ msec, $T1\rho_{Manual} \geq 55$ msec) groups were analyzed.

All tests were 2-tailed, with $P < 0.05$ considered statistically significant.

Results

Segmentation Time and Quality

The automated processing of T1ρ slices showed a marked significant reduction in processing time compared to manual processing in the testing set (~3 seconds vs. 1 minute 51 seconds ± 22 seconds). Figure 2 shows example LV segmentations and right ventricular insertion points generated by the proposed automated pipeline in seven patients presenting diverse cardiomyopathies. Figure S2 in the Supplemental Material shows the epicardial and endocardial contours obtained in four patients using the automated pipeline alongside those delineated by the two observers. The quality of LV

segmentation in the basal slices was significantly better than that in the apical slices, as evidenced by the significantly higher Dice and Jaccard indices (Table S2 in the Supplemental Material). Automated segmentation closely approximated the average of results obtained by the two annotators (global Dice of 81.9% ± 9.0 and global Jaccard index of 70.2% ± 12.0), and closely aligned with interobserver segmentation (global Dice 82.2% ± 6.5, $P = 0.97$, and global Jaccard index 70.2% ± 9.2, $P = 0.99$). Regarding manual LV wall volume segmentation, excellent intraobserver reproducibility (ICC = 0.96 [0.93–0.98]) and good interobserver reproducibility (ICC = 0.79 [0.65–0.88]; Fig. S3 in the Supplemental Material) was observed on a patient basis in the testing set with repeated segmentation (N = 47). Furthermore, when comparing LV wall volumes obtained through the automated pipeline with radiologist-derived volumes (global volume 29.3 cm^2 [26.3–36.7] vs. 29.7 cm^2 [25.4–36.7]; Table S3 in the Supplemental Material). There was a moderate to excellent ICC both at the patient level (Radiologist 1: 0.65 [0.46–0.79], Radiologist 2 Session 1: 0.91 [0.85–0.95]) and at the slice level (Radiologist 1: 0.72 [0.63–0.79], Radiologist 2 Session 1: 0.89 [0.85–0.92]; Table 2). When considering the entire testing cohort (N = 73), the ICC for LV wall volume segmentation further improved on a patient (0.94 [0.91–0.96]) and slice basis (0.93 [0.91–0.95]; Fig. S4 in the Supplemental Material) with minimal bias of −0.93 cm^2 (95% CI: −7.5 to 5.7 cm^2) and −0.31 cm^2 (95% CI: −3.2 to 2.6 cm^2), respectively.

Landmarks Precision

The accuracy of the LV center of mass is shown by the small distance observed between the automated pipeline and manual measurements (center of mass difference of 3.1 mm ± 2.4; Table S2 in the Supplemental Material), closely approximating interobserver error (2.7 mm ± 1.8, $P = 0.33$). The center of mass difference between manual and automated segmentation did not show significant variation between slices ($P = 0.578$). Furthermore, the distance between the identified right ventricular insertion points and the reference standard was small, with a slightly higher but significant discrepancy for the posterior point (5.5 mm [3.9–8.2] vs. 8.2 mm [6.4–10.8]; Fig. S5 in the Supplemental Material). There was also a small but significant difference for the angle (7.2° [3.6–11.6] vs. 11.5° [8.5–15.1]). The confidence score for detecting both landmarks in the testing set was 94.4% (95% CI: 91.3% to 95.7%). With the exception of the infero-apical and latero-apical segments, there were no significant differences in ROI size between automated and

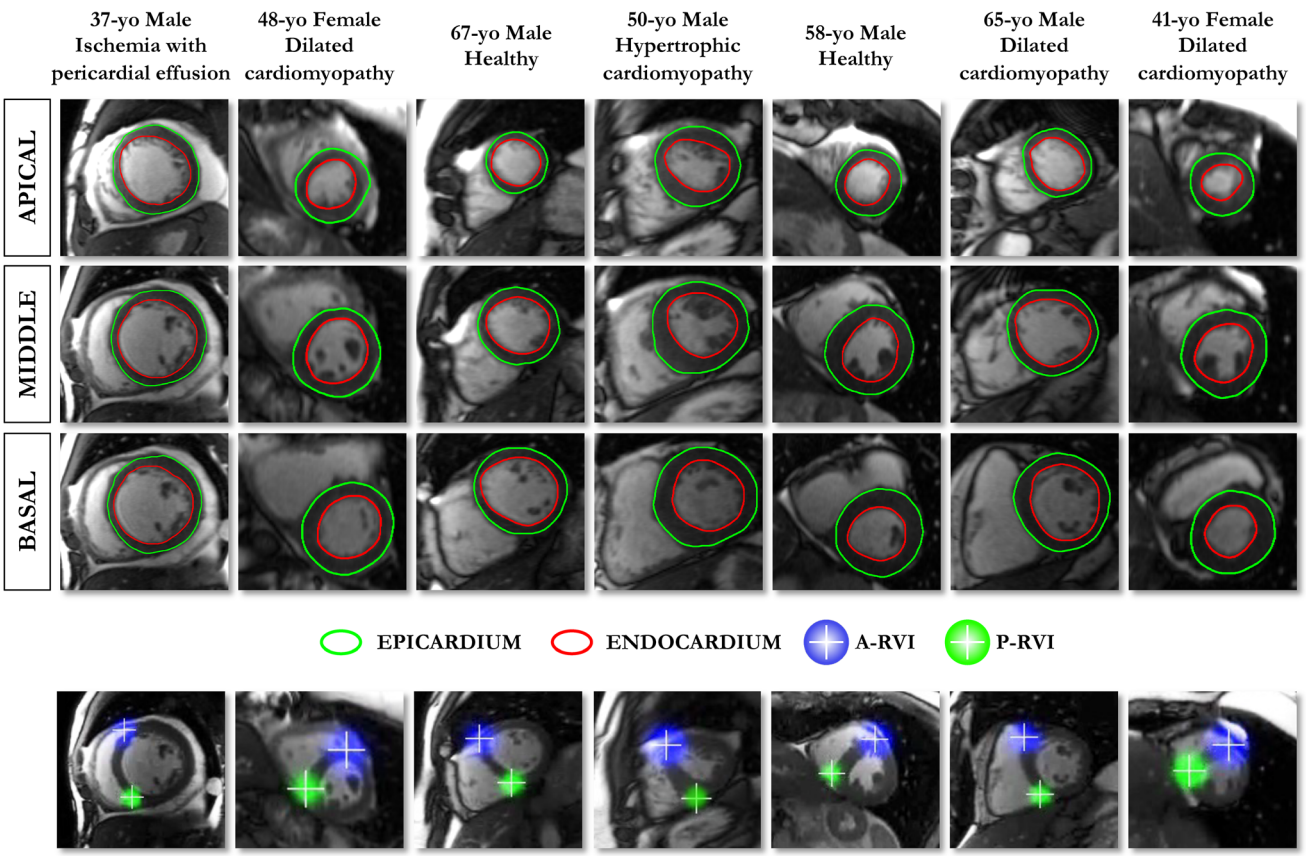

FIGURE 2: Automated pipeline results showcasing left ventricular segmentation outcomes (top) and identified right ventricular insertion points (bottom) in seven patients presenting diverse cardiomyopathies. LV = left ventricle; A-RVI = anterior right ventricular insertion point; P-RVI = posterior right ventricular insertion point.

TABLE 2. Intraclass Correlation Coefficient (ICC) With 95% Confidence Intervals for Left Ventricular Wall Volume, Comparing Automated and Manual Processing of Myocardial T1ρ Maps in 47 Patients

Left Ventricular Wall Volume Comparisons	ICC (95% Confidence Interval)	
	Patient Basis	Slice Basis
Radiologist 1—Radiologist 2 Session 1	0.73 [0.57–0.84]	0.78 [0.70–0.83]
Radiologist 1—Radiologist 2 Session 2	0.79 [0.65–0.88]	0.82 [0.76–0.87]
Radiologist 2 Session 1—Radiologist 2 Session 2	0.96 [0.93–0.98]	0.95 [0.93–0.96]
Automated—Radiologist 1	0.65 [0.46–0.79]	0.72 [0.63–0.79]
Automated—Radiologist 2 Session 1	0.91 [0.85–0.95]	0.89 [0.85–0.92]
Automated—Radiologist 2 Session 2	0.91 [0.84–0.95]	0.90 [0.87–0.93]
Automated—Average Radiologist 1 and Radiologist 2 Session 1	0.88 [0.79–0.93]	0.89 [0.85–0.92]

manual processing for each AHA segment (Table S4 in the Supplemental Material).

Myocardial T1ρ Reproducibility

In the test cohort, there was no significant difference in global myocardial T1ρ values between manual processing (54.9 msec ± 4.6; 95% CI: 53.8 to 56.0 msec, range: 46.6–70.9 msec) and automated processing (55.4 msec ± 5.1; 95% CI: 54.2 to 56.6 msec, range: 46.4–75.1 msec; $P = 0.099$; Table 3). The automated pipeline demonstrated a good level of agreement with radiologist-derived myocardial T1ρ values, with ICC of 0.85 (95% CI: 0.77 to 0.90), 0.80 (95% CI: 0.74 to 0.84), and 0.65 (95% CI: 0.62 to 0.68) at the patient, slice, and segment levels, respectively. Minimal biases and 95% limits of agreement were observed, with T1ρ differences of +0.52 msec ± 5.18, +0.78 msec ± 8.52, and +0.52 msec ± 14.48, respectively (Fig. 3). No significant differences in myocardial T1ρ values were found between the automated pipeline and manual processing across the 16 segments defined by the AHA (One-way ANOVA $P = 0.75$; Fig. 4a) or on individual slices (basal $P = 0.99$, middle $P = 1.00$, apical $P = 0.08$; Fig. 4b). A slight trend toward higher T1ρ values was observed in the apical segments for both automated and manual processing ($P < 0.001$). Average myocardial T1ρ values between the automated pipeline and manual processing across the different patient groups (MRI-negative, ischemic, myocarditis, hypertrophic cardiomyopathy, dilated cardiomyopathy, and Takotsubo) are shown in Table 4. Only the dilated cardiomyopathy group showed slightly but significantly higher T1ρ values with the automated pipeline compared to manual processing (56.2 msec ± 5.2 vs. 54.0 msec ± 3.8). Figure S6 in the Supplemental Material shows the results of the proposed framework in two MRI-negative subjects. Figure 5 shows the 16-segment AHA representations and corresponding contrast agent-free T1ρ maps for both manual and automated processing in two patients with ischemic and nonischemic heart disease. Figure 6 provides the same visual comparison for three patients with Takotsubo cardiomyopathy.

Identification of Patients With Elevated T1ρ Values

The fully automated framework provided robust diagnostic performance on a patient basis, with a sensitivity of 91.4% (95% CI: 81.9 to 96.8), a specificity of 89.5% (95% CI: 79.5 to 95.5), a positive predictive value of 88.9% (95% CI: 78.8 to 95.1), a negative predictive value of 91.9% (95% CI: 82.5 to 97.1), and an overall accuracy of 90.4% (95% CI: 80.7 to 96.1) for identifying abnormal T1ρ values (Table S5 in the Supplemental Material).

TABLE 3. Manual vs. Automated Extraction of Global Myocardial T1ρ Values in the Test Cohort (N = 73)

Global T1ρ (msec)	Mean ± SD	95% CI	[Min, Max]	Range Differences
Manual	54.9 ± 4.6	[53.8, 56.0]	[46.6, 70.9]	24.3
Automated	55.4 ± 5.1	[54.2, 56.6]	[46.4, 75.1]	28.7

SD = standard deviation; CI = confidence interval.

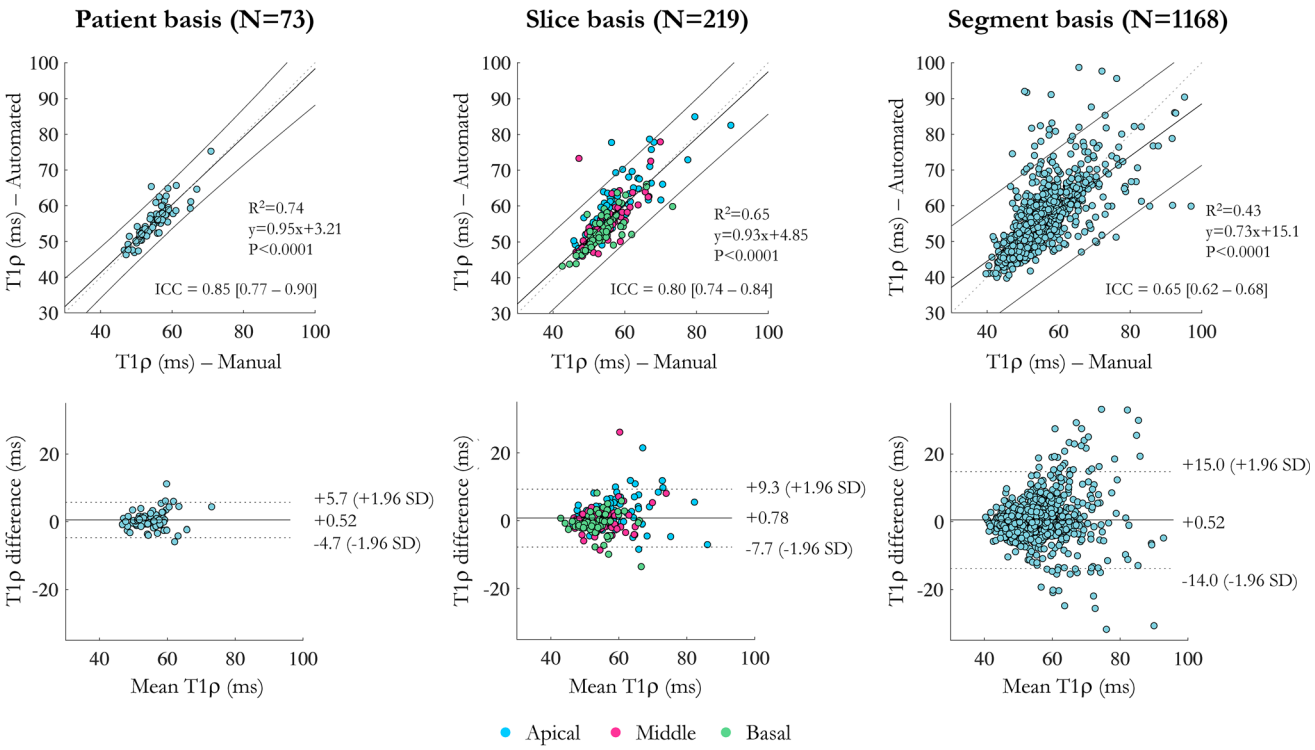

FIGURE 3: Bland–Altman analysis for myocardial T1ρ values derived from T1ρ maps comparing manual and fully automated processing on a patient (N = 73), slice (N = 219), and segment (N = 1168) basis.

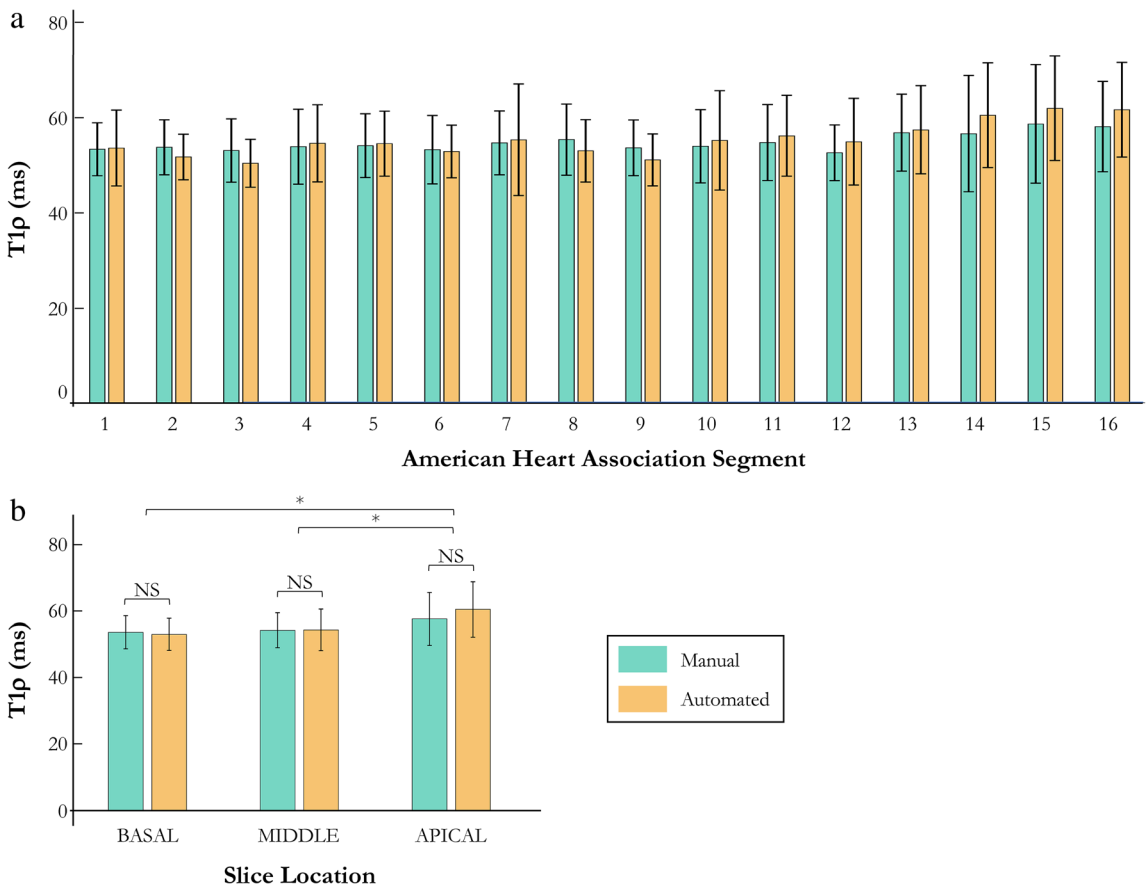

FIGURE 4: Myocardial T1ρ measurement in the 16 American Heart Association segments (a) and at basal, middle, and apical slice levels (b) obtained with manual and automated processing in a test cohort of 73 patients. Errors bars represent standard deviation. NS = non-significant, *P < 0.001.

Discussion

This study investigated the performance of an AI-based framework for the automated quantification of contrast agent-free myocardial T1ρ mapping in a clinical setting. First, the automated segmentation of LV contours on T1ρ-weighted images was shown to be feasible and reproducible, even with the relatively small training dataset. Second, this approach enabled accurate extraction of global and segmental myocardial T1ρ values in a fast and fully automated manner. Third, its seamless clinical integration not only resulted in substantial time savings compared to conventional manual methods but also has potential to enable real-time diagnosis of myocardial lesions during scanning. Taken together, this framework takes a step toward quicker, "needle-free," and more efficient management of patients with heart disease.

Automated Quantification of Myocardial Parameter Mapping

Several innovative approaches have emerged to automate the quantification of myocardial T1 mapping,[10,26–29] T2 mapping,[30] and the fusion of both.[11,31] In their respective studies, Kim et al,[30] Fahmy et al,[10] and Puyol-Antón et al[26] used U-Net and advanced U-Net architectures, meticulously trained on datasets comprising 586, 210, and 800 carefully selected subjects, respectively. Howard et al[31] adopted the deep high-resolution representation learning (HigherHRNet) framework, trained on a dataset of 713 patients for the automation of joint T1 and T2 mapping using the mSASHA sequence. This network has multiple advantages over the U-Net models, including finer and more spatially accurate segmentation.[31] By exploiting self-attention mechanisms, the transformer model employed in the current study has shown even better performance in medical image segmentation,[15] by capturing patterns and global spatial dependencies within the images and by improving computational efficiency. A comprehensive comparison of these segmentation architectures for MRI parameter mapping remains to be established.

In the current study, elevated T1ρ values were observed in the apical segments which might be attributed to their susceptibility to partial volume averaging, a phenomenon previously reported in T1 and T2 mapping.[32–34] The lower segmentation quality in the apical segment, as indicated by lower Dice and Jaccard indices, could also contribute to this. In the dilated cardiomyopathy group, T1ρ values were significantly higher with automated processing compared to manual processing. This discrepancy may be linked to thinner myocardial walls and diminished segmentation performance, as corroborated by the slightly lower Dice score.

Future study may include extending the proposed framework to other mapping techniques, including T1 and T2 mapping. Additionally, extending the framework to high-resolution 3D T1ρ mapping[35,36] may offer opportunities for various applications, such as atrial or right ventricular imaging. Lastly, conducting follow-up studies to assess the framework's results and performance over time is an avenue for future research.

Limitations

The single-center, single-scanner design and relatively small sample size in this study cannot eliminate center-specific and manufacturer-specific T1ρ bias. Additionally, a larger sample size is important to increase the performance of deep learning-based automated segmentation. Unfortunately, the absence of an open-access T1ρ dataset has hindered the use of deep learning in LV segmentation tasks. Furthermore, our test dataset lacked sufficient representation for each cardiomyopathy subtype, resulting in insufficient statistical power to achieve a robust comparison between manual and automated processing methods. A larger, more diverse cohort encompassing various heart conditions is essential to enhance the robustness of this study.

TABLE 4. Comparative Analysis of Global T1ρ Values Obtained From Manual and Automated Processing Pipelines in the Different Cardiomyopathies Within the Test Cohort

Cardiomyopathy	No. of Patients	Mean T1ρ Automated (msec)	Mean T1ρ Manual (msec)	*P*-Value	Global DICE (%)
MRI-negative	16	52.9 ± 5.6	50.9 ± 3.1	0.249	83 ± 5
Ischemic	13	57.5 ± 3.9	56.7 ± 3.0	0.482	83 ± 5
Myocarditis	8	59.3 ± 6.4	54.1 ± 3.0	0.229	81 ± 6
HCM	5	51.9 ± 1.7	51.2 ± 0.9	0.427	86 ± 4
DCM	25	56.2 ± 5.2	54.0 ± 3.8	0.027	82 ± 5
Takotsubo	6	67.4 ± 11.2	64.9 ± 8.4	0.427	84 ± 3

HCM = hypertrophic cardiomyopathy; DCM = dilated cardiomyopathy.

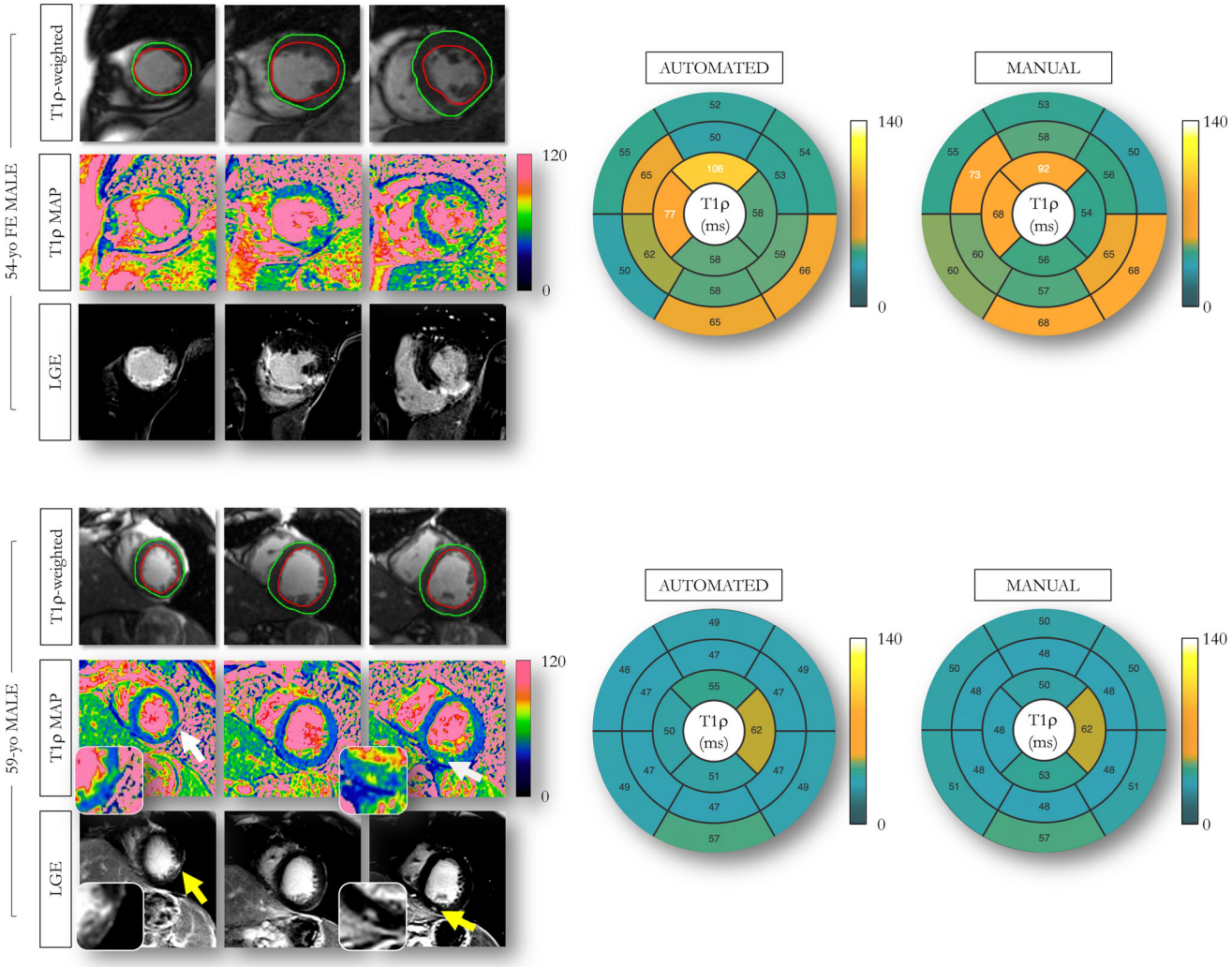

FIGURE 5: Comparison of 16-segment American Heart Association Bullseye representations and corresponding T1ρ maps, as well as T1ρ-weighted images (spin-lock time of 35 msec), for both manual and automated processing in a patient with ischemic heart disease (top row) and in a patient with both ischemic and nonischemic heart disease (bottom row). Post-contrast late gadolinium enhancement (LGE) images are also provided. Arrows highlight regions exhibiting elevated T1ρ values and hyperenhancement on LGE imaging.

Nevertheless, compared to previous studies, this study used a relatively large myocardial T1ρ mapping database and may benefit the wider research community. Furthermore, the framework's inline implementation holds promise for its deployment in external clinical centers for multicentric studies spanning diverse patient demographics.

This study did not measure and compare fibrotic extent and transmurality in ischemic and nonischemic cardiomyopathies against established LGE techniques, primarily due to the limited 3-slice short-axis coverage of the data collected. The algorithm implemented in the current study is designed to handle an arbitrary number of slices which would facilitate the assessment of T1ρ diagnostic accuracy in forthcoming studies.

Due to time and institutional constraints, the training dataset in the current study only comprised whole-heart TSL_{35} images. Improved segmentation accuracy could potentially be achieved by leveraging all T1ρ-weighted images using a multi-channel Swin Transformer architecture.[37] However, this will only be possible after the construction of sufficiently large registry. Our study employed an 85:15 train-test splitting scheme, but exploring alternative splits such as 80:20 or 75:25 may also mitigate the variability of performance estimates.

Remaining Hurdles for the Broad Clinical Integration of Myocardial T1ρ Mapping

Enhancements in spatial resolution is a crucial requirement for advancing clinical detection capabilities and facilitating finer differentiation of myocardial lesions. While myocardial T1ρ mapping is still in its early stages, the emergence of 3D applications, in Cartesian and non-Cartesian formats, have shown significant advancement.[35] The integration into a "free-running" framework may also be crucial in achieving

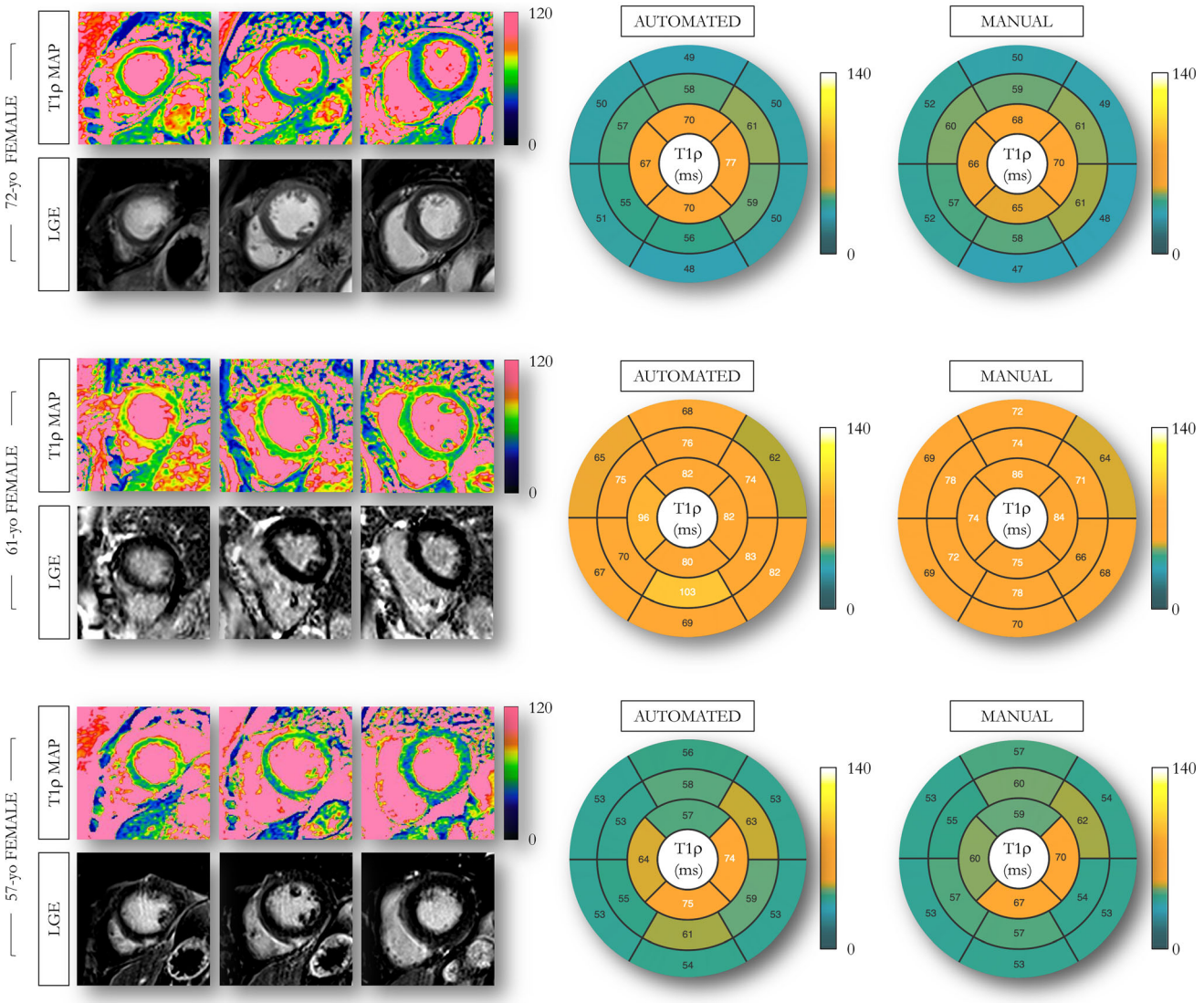

FIGURE 6: Comparison of 16-segment American Heart Association Bullseye representations and corresponding T1ρ maps for three patients with Takotsubo cardiomyopathy, analyzed both manually and via automated processing. Post-contrast late gadolinium enhancement (LGE) images are included for reference.

cardiac- and respiratory-resolved (5D) T1ρ mapping.[38] Its integration into a multiparametric mapping presents an opportunity for a comprehensive evaluation of myocardial tissue characteristics. Magnetic Resonance Fingerprinting (MRF), for example, promises the joint assessment of multiple parameters, thereby enabling a comprehensive examination. Velasco et al have introduced such framework facilitating simultaneous T1ρ, T1, and T2 cardiac mapping within a single 16-second scan.[39]

Furthermore, other artificial intelligence applications offer a spectrum of prospects, including quality control and motion correction, both directed toward alleviating manual workload and fostering clinical applicability.[9]

Nevertheless, the widespread clinical adoption of T1ρ mapping encounters challenges pertaining to standardization and transferability. Encouragement of collaborative endeavors and fostering the sharing of protocols, will help enhancing accessibility and standardization. Moreover, granting open access to data, reconstruction techniques, and code used for analysis may improve reproducibility and bring myocardial T1ρ mapping closer to routine clinical practice. Lastly, there is a lack of certainty regarding the nature of T1ρ tissue variations and whether they reliable indicate disease. This remains to be clinically validated in prospective and randomized trials.

Conclusion

Automated processing of myocardial T1ρ mapping demonstrated strong agreement with manual processing, and had greater time efficiency and comparable segmentation quality.

These results highlight its potential for conducting noninvasive, "needle-free," and rapid on-site assessment of structural heart disease.

Acknowledgments

This work was supported by funding from the French National Research Agency under grant agreements Equipex MUSIC ANR-11-EQPX-0030, Programme d'Investissements d'Avenir ANR-10-IAHU04-LIRYC, ANR-22-CPJ2-0009-01, and from the European Research Council (ERC) under the European Union's Horizon Europe research and innovation programme (Grant agreement 101076351).

References

1. Witschey WRT, Zsido GA, Koomalsingh K, et al. In vivo chronic myocardial infarction characterization by spin locked cardiovascular magnetic resonance. J Cardiovasc Magn Reson 2012;14(1):1-9. https://doi.org/10.1186/1532-429X-14-37.
2. Bustin A, Witschey WRT, Van Heeswijk RB, Cochet H, Stuber M. Magnetic resonance myocardial T1ρ mapping technical overview, challenges, emerging developments, and clinical applications. J Cardiovasc Magn Reson 2023;1:1-18. https://doi.org/10.1186/s12968-023-00940-1.
3. Han Y, Liimatainen T, Gorman RC, Witschey WRT. Assessing myocardial disease using T1ρ MRI. Curr Cardiovasc Imaging Rep 2014;7(2):1-9. https://doi.org/10.1007/s12410-013-9248-7.
4. Rudnick MR, Wahba IM, Leonberg-Yoo AK, Miskulin D, Litt HI. Risks and options with gadolinium-based contrast agents in patients with CKD: A review. Am J Kidney Dis 2021;77(4):517-528. https://doi.org/10.1053/j.ajkd.2020.07.012.
5. Damman K, Valente MAE, Voors AA, O'Connor CM, Van Veldhuisen DJ, Hillege HL. Renal impairment, worsening renal function, and outcome in patients with heart failure: An updated meta-analysis. Eur Heart J 2014;35(7):455-469. https://doi.org/10.1093/eurheartj/eht386.
6. Wang L, Yuan J, Zhang SJ, et al. Myocardial T1rho mapping of patients with end-stage renal disease and its comparison with T1 mapping and T2 mapping: A feasibility and reproducibility study. J Magn Reson Imaging 2016;44(3):723-731. https://doi.org/10.1002/jmri.25188.
7. Bustin A, Witschey WRT, van Heeswijk RB, Cochet H, Stuber M. Magnetic resonance myocardial T1-rho mapping: Technical overview, challenges, emerging developments, and clinical applications. J Cardiovasc Magn Reson 2023;25(1):34.
8. Schulz-Menger J, Bluemke DA, Bremerich J, et al. Standardized image interpretation and post processing in cardiovascular magnetic resonance: Society for Cardiovascular Magnetic Resonance (SCMR) Board of Trustees Task Force on Standardized Post Processing. J Cardiovasc Magn Reson 2013;15(1):1-19. https://doi.org/10.1186/1532-429X-15-35.
9. Ogier AC, Bustin A, Cochet H, Schwitter J, van Heeswijk RB. The road toward reproducibility of parametric mapping of the heart: A technical review. Front Cardiovasc Med 2022;9(May):876475. https://doi.org/10.3389/fcvm.2022.876475.
10. Fahmy AS, El-Rewaidy H, Nezafat M, Nakamori S, Nezafat R. Automated analysis of myocardial native T1 mapping images using fully convolutional neural networks. J Cardiovasc Magn Reson 2019;21(7):1-12.
11. Zhu Y, Fahmy AS, Duan C, Nakamori S, Nezafat R. Automated myocardial T2 and extracellular volume quantification in cardiac MRI using transfer learning–based myocardium segmentation. Radiol Artif Intell 2020;2(1):e190034. https://doi.org/10.1148/ryai.2019190034.
12. Bustin A, Toupin S, Sridi S, et al. Endogenous assessment of myocardial injury with single-shot model-based non-rigid motion-corrected T1 rho mapping. J Cardiovasc Magn Reson 2021;23(1):1-14. https://doi.org/10.1186/s12968-021-00781-w.
13. Kellman P, Arai AE, McVeigh ER, Aletras AH. Phase-sensitive inversion recovery for detecting myocardial infarction using gadolinium-delayed hyperenhancement. Magn Reson Med 2002;47(2):372-383. https://doi.org/10.1002/mrm.10051.
14. Dosovitskiy A, Beyer L, Kolesnikov A, et al. An image is worth 16 × 16 words: Transformers for image recognition at scale. ICLR 2021 – 9th International Conference on Learning Representations 2021.
15. Gao Y, Zhou M, Liu D, Yan Z, Zhang S, Metaxas DN. A data-scalable transformer for medical image segmentation: Architecture, model efficiency, and benchmark. 2022.
16. Shamshad F, Khan S, Zamir SW, et al. Transformers in medical imaging: A survey. Med Image Anal 2023;88(March):102802. https://doi.org/10.1016/j.media.2023.102802.
17. Piechnik SK, Ferreira VM, Lewandowski AJ, et al. Normal variation of magnetic resonance T1 relaxation times in the human population at 1.5 T using ShMOLLI. J Cardiovasc Magn Reson 2013;15(1):13. https://doi.org/10.1186/1532-429X-15-13.
18. Xue H, Artico J, Fontana M, Moon JC, Davies RH, Kellman P. Landmark detection in cardiac MRI by using a convolutional neural network. Radiol Artif Intell 2021;3(5):e200197. https://doi.org/10.1148/RYAI.2021200197.
19. Ronneberger O, Fischer P, Brox T. U-net: Convolutional networks for biomedical image segmentation. Med Image Comput Comput Assist Interv–MICCAI 2015;9351:234-241. https://doi.org/10.1007/978-3-319-24574-4_28.
20. Cerqueira MD, Weissman NJ, Dilsizian V, et al. Standardized myocardial segmentation and nomenclature for tomographic imaging of the heart: A statement for healthcare professionals from the cardiac imaging. Circulation 2002;105(4):539-542. https://doi.org/10.1161/hc0402.102975.
21. Selvadurai BSN, Puntmann VO, Bluemke DA, et al. Definition of left ventricular segments for cardiac magnetic resonance imaging. JACC Cardiovasc Imaging 2018;11(6):926-928. https://doi.org/10.1016/j.jcmg.2017.09.010.
22. Hansen MS, Sørensen TS. Gadgetron: An open source framework for medical image reconstruction. Magn Reson Med 2013;69(6):1768-1776. https://doi.org/10.1002/mrm.24389.
23. Koo TK, Li MY. A guideline of selecting and reporting intraclass correlation coefficients for reliability research. J Chiropr Med 2016;15(2):155-163. https://doi.org/10.1016/j.jcm.2016.02.012.
24. Dice LR. Measures of the amount of ecologic association between species. Ecology 1945;26:297-302. https://doi.org/10.2307/1932409.
25. Jaccard P. The distribution of the flora in the alpine zone. New Phytol 1912;11(2):37-50.
26. Puyol-Antón E, Ruijsink B, Baumgartner CF, et al. Automated quantification of myocardial tissue characteristics from native T1 mapping using neural networks with uncertainty-based quality-control. J Cardiovasc Magn Reson 2020;22(1):1-15. https://doi.org/10.1186/s12968-020-00650-y.
27. Farrag NA, Lochbihler A, White JA, Ukwatta E. Evaluation of fully automated myocardial segmentation techniques in native and contrast-enhanced T1-mapping cardiovascular magnetic resonance images using fully convolutional neural networks. Med Phys 2021;48(1):215-226. https://doi.org/10.1002/mp.14574.
28. Viezzer D, Hadler T, Ammann C, et al. Introduction of a cascaded segmentation pipeline for parametric T1 mapping in cardiovascular magnetic resonance to improve segmentation performance. Sci Rep 2023;13(1):1-14. https://doi.org/10.1038/s41598-023-28975-5.
29. Bhatt N, Ramanan V, Orbach A, et al. A deep learning segmentation pipeline for cardiac T1 mapping using MRI relaxation–based synthetic contrast augmentation. Radiol Artif Intell 2022;4(6):1-9. https://doi.org/10.1148/ryai.210294.

30. Kim H, Yang YJ, Han K, et al. Validation of a deep learning-based software for automated analysis of T2 mapping in cardiac magnetic resonance imaging. Quant Imaging Med Surg 2023;13(10):6750-6760. https://doi.org/10.21037/qims-23-375.

31. Howard JP, Chow K, Chacko L, et al. Automated inline myocardial segmentation of joint T1 and T2 mapping using deep learning. Radiol Artif Intell 2023;5(1):1-10. https://doi.org/10.1148/ryai.220050.

32. Bönner F, Janzarik N, Jacoby C, et al. Myocardial T2 mapping reveals age- and sex-related differences in volunteers. J Cardiovasc Magn Reson 2015;17(1):1-11. https://doi.org/10.1186/s12968-015-0118-0.

33. Wassmuth R, Prothmann M, Utz W, et al. Variability and homogeneity of cardiovascular magnetic resonance myocardial T2-mapping in volunteers compared to patients with edema. J Cardiovasc Magn Reson 2013;15(1):1-10. https://doi.org/10.1186/1532-429X-15-27.

34. Von Knobelsdorff-Brenkenhoff F, Prothmann M, Dieringer MA, et al. Myocardial T1 and T2 mapping at 3 T: Reference values, influencing factors and implications. J Cardiovasc Magn Reson 2013;15(1):1. https://doi.org/10.1186/1532-429X-15-53.

35. Qi H, Bustin A, Kuestner T, et al. Respiratory motion-compensated high-resolution 3D whole-heart T1ρ mapping. J Cardiovasc Magn Reson 2020;22(1):1-13. https://doi.org/10.1186/s12968-020-0597-5.

36. Kamesh IS, Moon B, Hwuang E, et al. Accelerated free-breathing 3D T1ρ cardiovascular magnetic resonance using multicoil compressed sensing. J Cardiovasc Magn Reson 2019;21(1):1-11. https://doi.org/10.1186/s12968-018-0507-2.

37. Liu Z, Lin Y, Cao Y, et al. Swin transformer: Hierarchical vision transformer using shifted windows. Proceedings of the IEEE International Conference on Computer Vision2021:9992–10002. https://doi.org/10.1109/ICCV48922.2021.00986.

38. Di Sopra L, Piccini D, Coppo S, Stuber M, Yerly J. An automated approach to fully self-gated free-running cardiac and respiratory motion-resolved 5D whole-heart MRI. Magn Reson Med 2019;82(6):2118-2132. https://doi.org/10.1002/mrm.27898.

39. Velasco C, Cruz G, Lavin B, et al. Simultaneous T1, T2, and T1ρ cardiac magnetic resonance fingerprinting for contrast agent–free myocardial tissue characterization. Magn Reson Med 2022;87(4):1992-2002. https://doi.org/10.1002/mrm.29091.